International Journal of Marine Engineering Innovation and Research, Vol. 10(3), Sept. 2025. 795-811
(pISSN: 2541-5972, eISSN: 2548-1479)

Fatigue Analysis of Mid-Water Buoy (MWB) due to Changes in Pipeline End Manifold (PLEM) Position

Ibrahim Rahmatulloh[1], Handayanu [2], Nur Syahroni [3]
(Received: 31 July 2025 / Revised: 12 August 2025 /Accepted: 12 August 2025 / Available Online: 6 September 2025)

***Abstract*— This research is a case study of the Mid-Water Buoy (MWB) structure on the subsea hose string SPM #4 after the installation of New PLEM C, or in other words in conditions where the subsea hose string (including MWB) has been connected to New PLEM C. MWB is one of the ancillary components of the subsea hose string, which has the main function as a buoy to keep the entire subsea hose string at a safe distance to the seabed. By replacing the old PLEM-C with the New PLEM-C, the dynamic motion of the subsea hose when connected to the New PLEM-C will also be different compared to the dynamic motion when connected to the old PLEM-C. The objective of this study is to analyze the fatigue life of the MWB structure after the use of New PLEM-C. As the main input for fatigue analysis, cyclic load analysis acting on the MWB structure is carried out based on a deterministic approach through time domain simulation and continued with the calculation of the number of cycles with the rainflow cycle counting method. For local stress analysis in the critical area of the MWB structure, the hotspot stress method is carried out through the Finite Element Method (FEM) which refers to DNV-RP-C203. Furthermore, the fatigue life calculation is carried out by applying the Palmgren-Miner rules and utilizing the S-N Curve. From a series of analyses that have been carried out it was found that the lowest fatigue life value for the MWB structure is occurs at PART B1 (the part of the MWB connected to the Subsea Hose STRING B – Upper) with a value of 145.93 years and with an annual damage ratio of 0.0069 for the Connection between the Vertical Stiffener and the Pipe.**

Keywords— Mid-Water Buoy, Fatigue Analysis, Cumulative Damage, Hotspot Stress, Rainflow Counting.

I. INTRODUCTION

Indonesia, as one of the largest oil and gas producing countries in Southeast Asia [1], [2], has various strategic facilities needed to support oil and gas production, storage and distribution activities. One such strategic facility is the Ardjuna Marine Terminal, located in offshore of Java Sea (approximately 50 km north of Karawang and Subang Cities). This terminal serves as a strategic point in the crude oil distribution chain, specifically supporting the transportation of crude oil to domestic and international markets.

To support the loading and offloading activities, the Ardjuna Marine Terminal has two main facilities, which are 2 (two) Single Point Mooring (SPM), namely SPM #3 and SPM #4. SPM #3 functions as a mooring facility for FSO, while SPM #4 functions as a mooring facility for Export Tankers when lifting (offloading) activities are in progress. Under normal operating conditions, the crude oil from the Flow Station will be sent to the FSO via a subsea pipeline and then forwarded through the subsea hose and floating hose, which is connected to SPM #3. Furthermore, for the offloading process, the crude oil will be pumped from the FSO through subsea pipelines and then forwarded through the subsea hose and floating hose of SPM #4, and finally, the crude oil will be received by the Export Tanker, which has been moored at SPM #4.

In 2022–2024, to enhance the integrity and reliability of the terminal facilities, the owner carried out an infrastructure renewal project at the Ardjuna Marine Terminal. This renewal included the replacement of all subsea pipelines and all Pipeline End Manifolds (PLEMs) at the Ardjuna Marine Terminal. Among the various activities undertaken, one of the key aspects highlighted in this study is the replacement of the Mid-Water Buoy (MWB) and the replacement of the old PLEM C with the New PLEM C located at SPM #4.

MWB have been used as alternative to distributed buoyancy systems in subsea hoses designs [3]. MWB has the main function as a floater to keep the entire series of subsea hoses at a safe distance (clearance distance) to the seabed. By replacing the old PLEM C with the New PLEM C, the motion of the subsea hose when connected to the New PLEM C will also be different compared to the motion when connected to the old PLEM C.

Based on the explanation above, this research will conduct a fatigue analysis of the MWB structure by applying the deterministic approach and the hotspot stress method. The analysis carried out in this study will include mooring lines and marine hoses modelling, cyclic load analysis, local stress analysis by hotspot stress method through the Finite Element Method (FEM), and fatigue life calculation based on Palmgren-Miner Rules, utilizing the S-N Curve. The results of this study are expected to be a technical reference and

Ibrahim Rahmatulloh, Department of Ocean Engineering, Institut Teknologi Sepuluh Nopember, Surabaya, 60111, Indonesia E-mail : ibrahimr.ibbi@gmail.com
Handayanu, Department of Ocean Engineering, Institut Teknologi Sepuluh Nopember, Surabaya, 60111, Indonesia E-mail : handayanu@oe.its.ac.id
Nur Syahroni, Department of Ocean Engineering, Institut Teknologi Sepuluh Nopember, Surabaya, 60111, Indonesia E-mail : nsyahroni@oe.its.ac.id

operational consideration material at Ardjuna Marine Terminal.

II. METHOD

This research is a case study which will analyze the fatigue life of the Mid-Water Buoy (MWB) structure on the subsea hose string of SPM #4 after the installation of New PLEM C, or in other words under conditions when the subsea hose string and MWB are connected to New PLEM C. Fatigue analysis for MWB structures will be carried out using a deterministic approach and the hotspot stress method.

A. Motion Response in Free Floating Condition

The research begins with 3D hull surface modeling for floating structures, which in this case are SPM #4 and Export Tanker. The SPM #4 and Export Tanker data used in the research can be seen in the Table 1 and Table 2. The results of the modeling have been validated by comparing the hydrostatic properties of the model output with the hydrostatic properties of existing data with acceptance criteria referring to [4].

The model will then be used to analyze the motion response under free-floating conditions. The output of this motion response analysis will be hydrodynamic properties, which will later be used as input for SPM #4 and the Export Tanker in modeling the overall mooring system and marine hoses.

The motion response of a floating structure consists of six degrees of freedom (6 DOF), assuming that the oscillatory movements are linear and harmonic, then the differential equation of the couple motion can be written as follows [5]:**TABLE 1.TABLE 1.**

$$\sum_{n=1}^{6}[(\boldsymbol{M_{jk}}+\boldsymbol{A_{jk}})\ddot{\xi}_k+\boldsymbol{B_{jk}}\dot{\xi}_k+\boldsymbol{K_{jk}}\xi_k=\boldsymbol{F_j}e^{i\omega t}\;;\; \boldsymbol{j,k=1\ldots.6} \quad (1)$$

Where:

$\boldsymbol{M_{jk}}$ = matrix of masses and moments of inertia of the floating structure.

$\boldsymbol{A_{jk}}$ = matrix of hydrodynamic added mass coefficients.

$\boldsymbol{B_{jk}}$ = matrix of hydrodynamic damping coefficients.

$\boldsymbol{K_{jk}}$ = matrix of stiffness coefficients or hydrostatic forces and moments.

$\boldsymbol{F_j}$ = matrix of excited forces and excited moments in complex functions (denoted by $\boldsymbol{e^{i\omega t}}$)

The complete process and method for the above modeling are not provided in this study, but are similar to [6].

B. Mooring System and Marine Hoses Modeling

Modeling for entire mooring lines and marine hoses will refer to the actual configuration in the field, which is shown in the following Figure 1. The Figure 1 shows the conditions when offloading activities are taking place, where an export tanker is moored at SPM #4. When offloading activities are not taking place, there are no ships moored at SPM #4, or what is then referred to as a buoy stand-alone condition.

SPM #4 is moored to the seabed with 6 (six) anchor chains, while the Export Tanker is moored to SPM #4 with 2 (two) mooring hawsers.

Each mooring line influences the system's load response based on its individual position, speed, and acceleration. The static analysis of the mooring lines was performed using the catenary method [7], [8], [9]. As referenced from [10], the catenary equation applied is shown in equation (2), where x denotes the segment length of the mooring line, H represents the horizontal component of the tension (a constant), y is the vertical component of the tension, and w is the weight per unit length.

$$y=\frac{H}{W}\left[\cosh\left(w\frac{x}{H}\right)-1\right] \quad (2)$$

TABLE 1.
PRINCIPAL PARTICULAR OF SPM #4

Parameter	Value
Deck House Diameter	9.00 m
Buoy Hull Diameter	12.00 m
Turret Tube Diameter	3.95 m
Outer Skirt Diameter	15.80 m
Deck House Height (incl. railing)	4.40 m
Buoy Hull Height	4.20 m
Turret Height (from Buoy Hull Bottom)	0.90 m
Turret to Spider Height	1.00 m
Overall Height	10.50 m
Installed Draft	±4.50 m
Mooring Configuration	6 x 1 leg
Number of Watertight Compartments	9
Approx. Weight	241.5 Ton

TABLE 2.
PRINCIPAL PARTICULAR OF EXPORT TANKER

Parameter	Value
Length over all (L_{OA})	251.51 m
Length Between Perpendicular (L_{PP})	239.00 m
Breadth (B)	43.80 m
Height (H)	21.30 m
Full Load Draft (T_{FULL})	15.04 m
Trim	0.00 m
Lightship Weight (Δ_{LIGHT})	20949.40 Ton
Deadweight (DWT)	113552.90 Ton
Full Load Displacement (Δ_{FULL})	134502.30 Ton

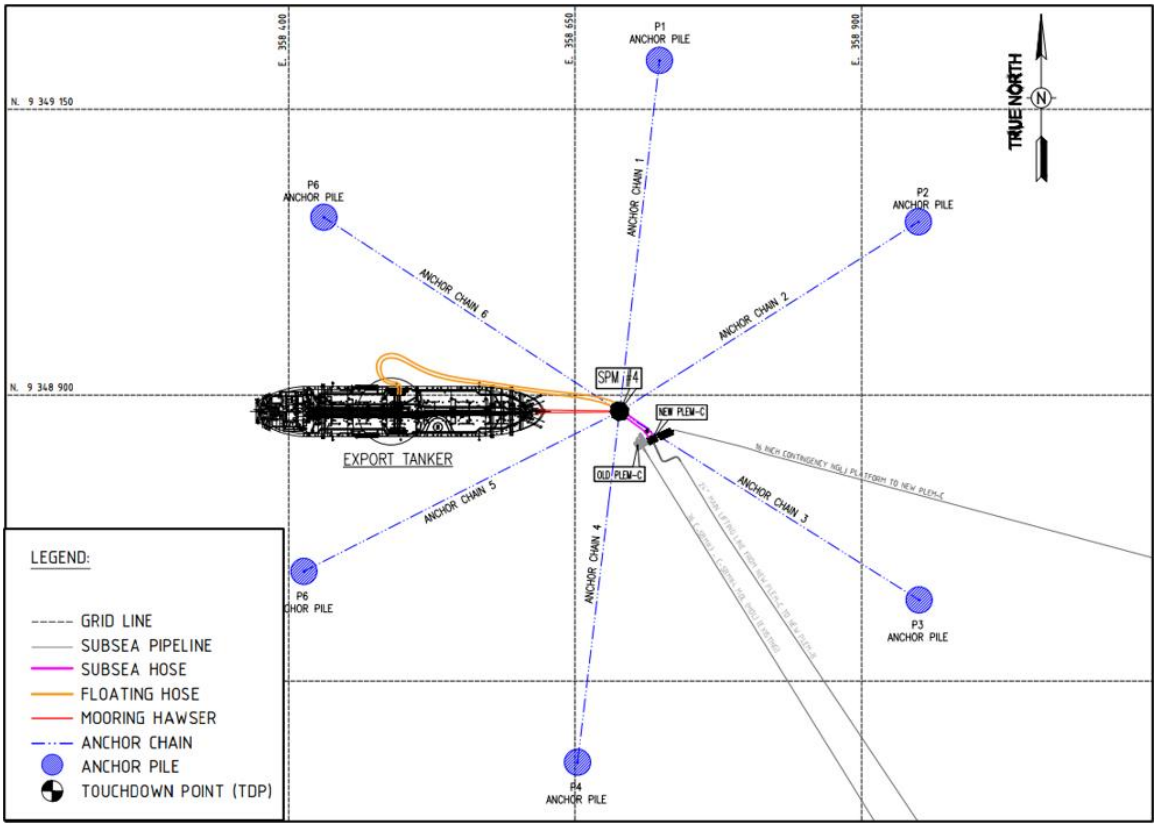

Figure 1. Existing Mooring System and Marine Hoses Configuration

Figure 1 also shows that 2 (two) strings of subsea hose are installed between SPM #4 and New PLEM C, and also 2 (two) strings of floating hose are installed between SPM #4 and Export Tanker. The complete configuration of the subsea hose can be seen in the Figure 2 and Table 3. The floating hose configuration is not shown in this study.

Referring to [11], the modeling of mooring lines applies line theory, with a lumped mass model. For marine hoses, the modeling is also done by applying line theory with a massless approach with distributed concentrated mass. In principle, the line element supports the flexibility of the line to experience axial displacement, torsion, tension and bending.

As illustrated in the Figure 2 and Table 3, the subsea hose configuration employed is the Lazy-S type, with an MWB installed on both hose strings. The MWB serves as the primary focus of this study. The MWB are utilized in subsea hose systems to achieve a Lazy-S configuration [12], [13]. An MWB is also classified as a subsea buoy, consisting of a pressure vessel filled pressure vessel filled with gas at ambient or higher pressure that gives uplift to the system [14]. The construction drawing and design parameter of MWB can be seen in Figure 3 and Table 4.

In this study, MWB was modelled as a lumped 6D buoy, which is considered as a rigid body with 6 degrees of freedom [15]. The required input properties for the buoy comprise of geometry, mass, volume and hydrodynamic coefficients. The hydrodynamic coefficients of MWB are calculated using the given data for simple shapes, such as cylinders, cubes, and spheres from [16].

The MWB is connected to subsea hose string using flange-to- flange connection. Therefore, in the modeling, each end connection of the subsea hose will be connected to the MWB, while the MWB itself will be set free, hence it can reflect the actual conditions of the motion dynamics between the MWB and the subsea hose.

C. Cyclic Load Analysis for MWB

As explained above, the MWB experiences dynamic and repetitive tension from the subsea hose, which is consistent with variations in environmental and operational conditions. Therefore, an analysis capable of depicting the actual cyclic loads experienced by the MWB is required. To accurately obtain these cyclic loads, a comprehensive analysis of the mooring system is necessary. In this study, the analysis was conducted based on time domain simulation to capture the dynamics of continuous loading. The model used in the time domain simulation encompasses all major components of the terminal, including SPM #4, the export tanker, anchor chain, mooring hawser, floating hose, subsea hose, and the MWB itself. The time domain simulation solves the general equations of motion for the combined mean, low, and wave frequency responses for all major components as mentioned above [17].

The analysis scenario is based on wave scatter data to depict annual wave statistics and serve as the basis for developing environmental load combinations. The environment data that used in this study can be seen in Table 5 and Table 6.

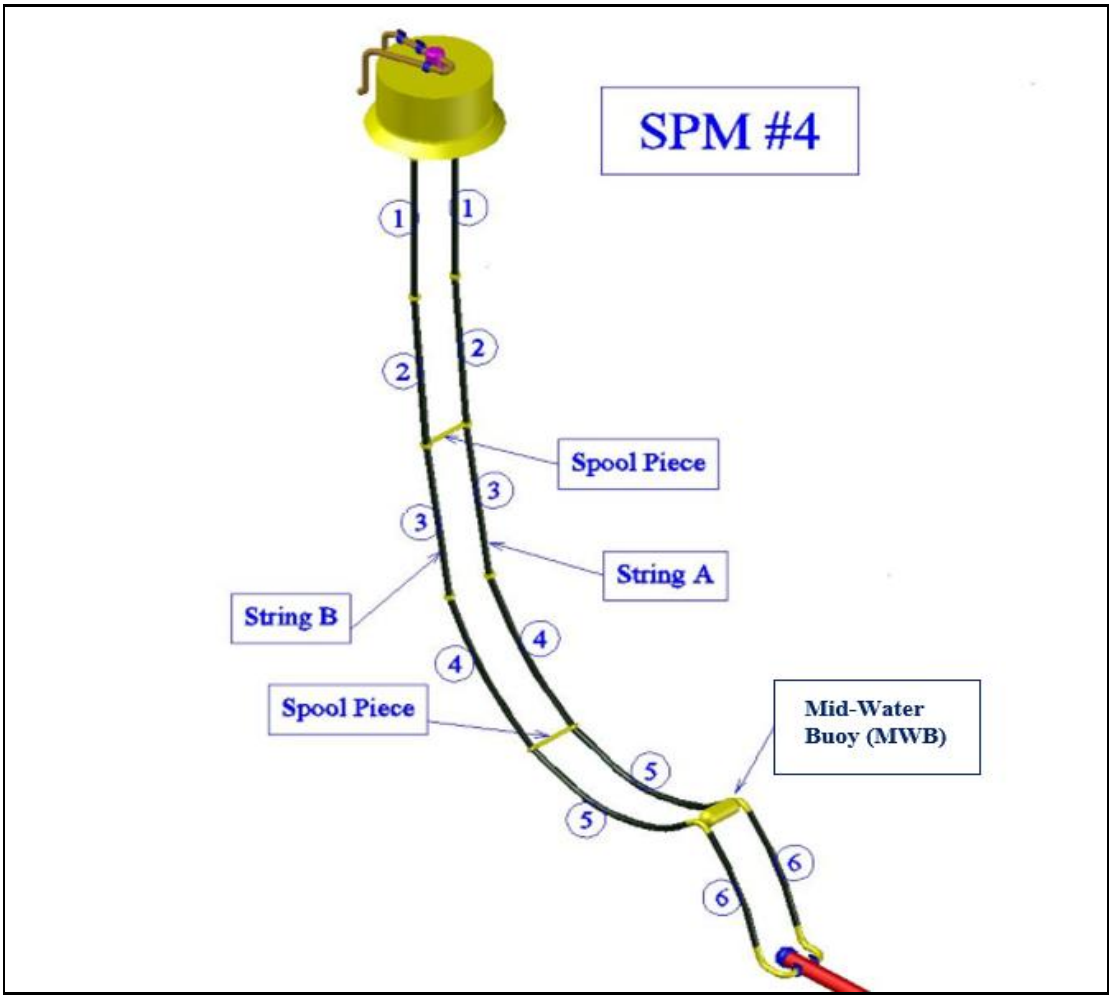

Figure 2. Illustration of Subsea Hose Configuration

TABLE 3
SUBSEA HOSE CONFIGURATION

FLOATING DEVICES		SPM #4	
Hose Part No	Description	String A	String B
1	Size	16" x 35 ft.	16" x 35 ft.
	Type	Full Length Reinforced Submarine Hose	Full Length Reinforced Submarine Hose
2	Size	16" x 35 ft.	16" x 35 ft.
	Type	Submarine Line Hose	Submarine Line Hose
3	Size	16" x 35 ft.	16" x 35 ft.
	Type	Submarine Line Hose	Submarine Line Hose
4	Size	16" x 35 ft.	16" x 35 ft.
	Type	Submarine Line Hose	Submarine Line Hose
5	Size	16" x 35 ft.	16" x 35 ft.
	Type	Full Length Reinforced Submarine Hose	Full Length Reinforced Submarine Hose
		MID-WATER BUOY (MWB)	
6	Size	16" x 35 ft.	16" x 35 ft.
	Type	Full Length Reinforced Submarine Hose	Full Length Reinforced Submarine Hose
SUBSEA DEVICES		PLEM-C	

Furthermore, to adapt to actual operating conditions, the analysis includes two main operational scenarios: when the export tanker is conducting lifting operations (normal lifting operation) and when there is no vessel moored to SPM #4 (buoy stand-alone condition). These two scenarios are important to consider as it gives different impacts on the dynamics of the subsea hose and the loads applied to the MWB.

The primary output of the time domain simulation will be time history data for tension of the subsea hose at the point of interaction with the MWB. This data illustrates the loads applied to the MWB over time due to the dynamic motions of all major components as mentioned above. This time history data is then processed using the rainflow cycle counting method to identify and calculate the number of loading cycles based on the tension range and frequency, thus obtaining a distribution of the number of cycles per year. These results will later be used as input in calculating the hotspot stress and fatigue life of the MWB Structure.

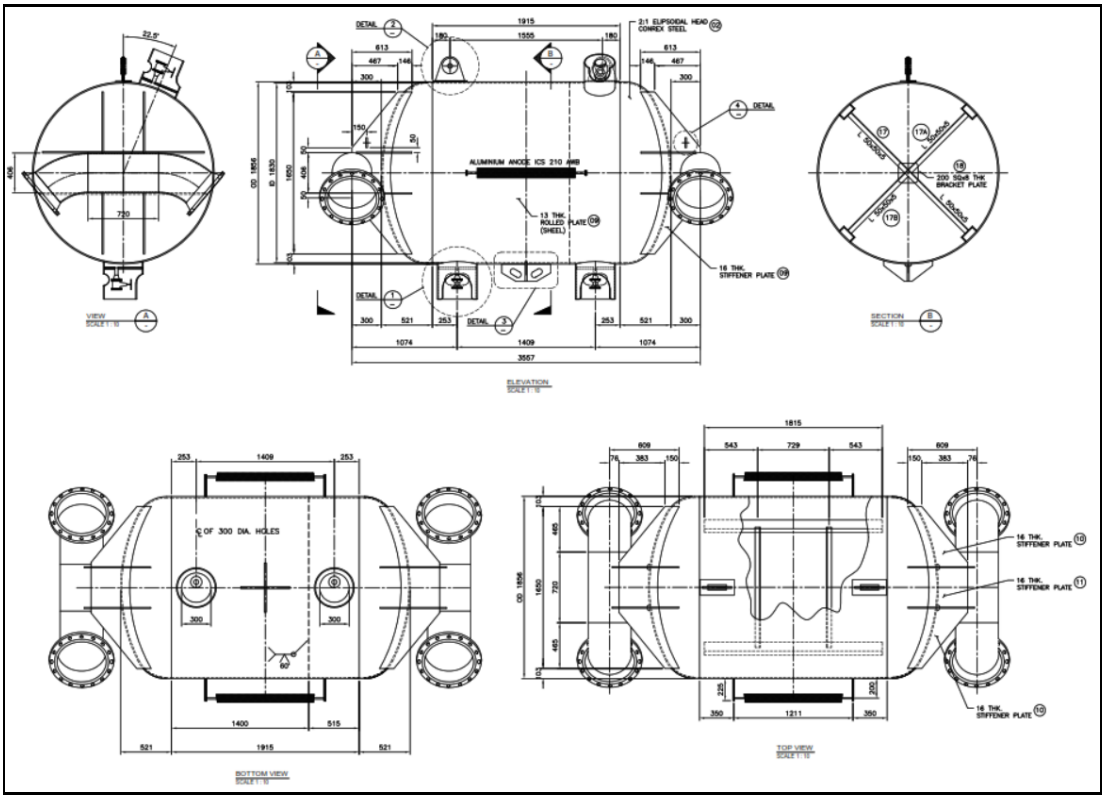

Figure 3. Construction Drawing of Mid-Water Buoy (MWB)

TABLE 4.
DESIGN PARAMETER OF MID-WATER BUOY (MWB)

Parameter		Value	Unit
Pressure	Design	0.800	MPa
	MAOP	0.517	MPa
Total Weight		3382.14	Kg
Volume	Cylinder Body	5.04	m^3
	Elipsoidal Head	1.90	m^3
	MWB (Moulded)	6.94	m^3
Buoyancy	Reserve Buoyancy	7112.70	Kg
	Net Buoyancy	3730.56	Kg

The rainflow cycle counting method is now generally regarded as the method leading to the best estimators of fatigue life [18], [19], [20]. Figure 4 shows the procedure for the cycle counting method as demonstrated by [21].

(i) Consider a sequence comprising alternating peaks and valleys, where point A denotes the most recent data point, point B the preceding one, and so forth. The range from point A to B is greater than that from point B to C.

(ii) Given that the range between A and B exceeds that between B and C, this indicates the completion of a cycle, which is defined by the interval from point B to point C.

(iii) As illustrated in Figure 4 (b), a new cycle emerges. Consistent with the previous pattern, the range from A to B surpasses that from B to C, thereby designating the B–C segment as a complete cycle. This process is iteratively applied until no further cycles can be identified at the current step.

The detail algorithm to implement the above procedure are referring to [22].

D. Local Structure Modeling of MWB

Local modeling was conducted to evaluate the structural behavior of the MWB in greater detail, particularly in areas considered critical due to stress concentrations or potential material fatigue. This local analysis is crucial for providing a more accurate depiction of the structure's response to operational and environmental loads, particularly after system configuration changes such as the relocation of the PLEM

TABLE 5.
ENVIRONMENT CONDITION DATA

Parameter	Unit	Return Period	
		1-year	100-year
Average Water Depth	m	43.00	
Wind Speed	m/s	12.30	25.70
Current Speed at Surface	m/s	0.72	1.15

TABLE 6.
WAVE SCATTER DATA

Individual Wave Height (m)	Direction (FROM)									
	N	NE	E	SE	S	SW	W	NW	SUM	C. SUM
0.00 - 0.25	271.2	215.5	1619.5	461.1	177.6	120.5	223.9	501.2	3590.4	3590.4
0.25 - 0.50	176.3	108.9	1521.5	216.0	68.6	73.2	226.9	531.4	2922.6	6513.1
0.50 - 0.75	48.6	23.1	760.2	50.4	11.4	18.6	105.9	282.0	1300.3	7813.3
0.75 - 1.00	12.4	4.7	341.2	11.1	1.4	3.8	41.6	131.4	547.6	8361.0
1.00 - 1.25	3.7	1.2	148.2	2.7	0.1	0.7	15.4	60.6	232.7	8593.7
1.25 - 1.50	1.4	0.4	63.1	0.8		0.2	5.7	28.2	99.7	8693.4
1.50 - 1.75	0.6	0.1	26.5	0.2		0.1	2.1	13.4	43.1	8736.5
1.75 - 2.00	0.3		11.1	0.1			0.8	6.4	18.7	8755.3
2.00 - 2.25	0.2		4.6				0.3	3.1	8.2	8763.5
2.25 - 2.50	0.1		1.9				0.1	1.6	3.7	8767.1
2.50 - 2.75	0.1		0.8				0.1	0.8	1.7	8768.7
2.75 - 3.00			0.3					0.4	0.8	8769.5
3.00 - 3.25			0.1					0.2	0.4	8769.9
3.25 - 3.50								0.1	0.2	8770.1
3.50 - 3.75								0.1	0.1	8770.1
3.75 - 4.00										8770.2
SUM	514.9	354.0	4498.9	742.4	259.1	217.0	622.9	1560.9	8770.2	

Note: the numbers in the table multiplied by 1000 gives the number of waves per year for each height and direction bin.

In the context of this study, local modeling begins with the identification of critical areas based on the results of the global analysis and structural design considerations of the MWB. Next, 3D geometry was developed for the identified areas using appropriate modeling software. Once the geometry was prepared, the next stage was the meshing process, in which the model was divided into smaller elements for numerical analysis using the finite element method (FEM).

E. Hotspot Stress Calculation

Hotspot stress analysis was conducted to evaluate local stresses in critical areas of the MWB structure that are potentially susceptible to fatigue failure. In this study, the hotspot stress methods were chosen as they are considered capable of accounting for stress concentrations in joints or complex geometries, particularly welds, and other structural element junctions that cannot be accurately represented by nominal stress.

The hotspot stress analysis process begins with the determination of load cases that represent the environmental and operational conditions most critical to the structure's response. Next, stress read-out points are selected on the surface of the critical area of the MWB structure at predetermined hotspot and notch positions, in accordance with standard guidelines, in this case the standard used is [23]. The stress results at these points are then analyzed to identify the magnitude of the hotspot stresses that occur, which are then used in the fatigue life calculation.

For hotspot stress analysis, the stress evaluation point is recommended at distances of 0.5 t and 1.5 *t* from the hotspot, where *t* is the plate thickness at the weld end. These locations are also denoted as stress read-out points. For more details, see Figure 5.

Refer to [23], the effective hotspot stress range that will be used in conjunction with the hotspot S-N curve is derived below:

$$\sigma_{eff} = \max \begin{cases} \sqrt{\Delta\sigma_{\perp}^2 + \Delta\tau_{\parallel}^2} \\ \alpha|\Delta\sigma_1| \\ \alpha|\Delta\sigma_2| \end{cases} \quad (3)$$

Where:
α = 0.90 if the weld type is classified as class C2.
α = 0.80 if the weld type is classified as class C1.
α = 0.72 if the weld type is classified as class C.
$\Delta\sigma$ = Principal stress range.

F. Fatigue Life Calculation

The fatigue life calculation for MWB structure will be carried out using the deterministic method with the S-N Curve approach. The deterministic method has been performed for many years and has proven to be a reliable approach for fatigue life analysis [24].

Meanwhile, the S-N curve used in this study is based on [23], which is described by the following equation:

$$\log N = \log \bar{a} - m \log \Delta\sigma \quad (4)$$

Where:
N = Predicted number of cycles to failure for the stress range Δσ.
$\Delta\sigma$ = Stress range.
m = Negative inverse slope of the S-N curve.
$\log \bar{a}$ = Intersection of the log N axis with the S-N curve.

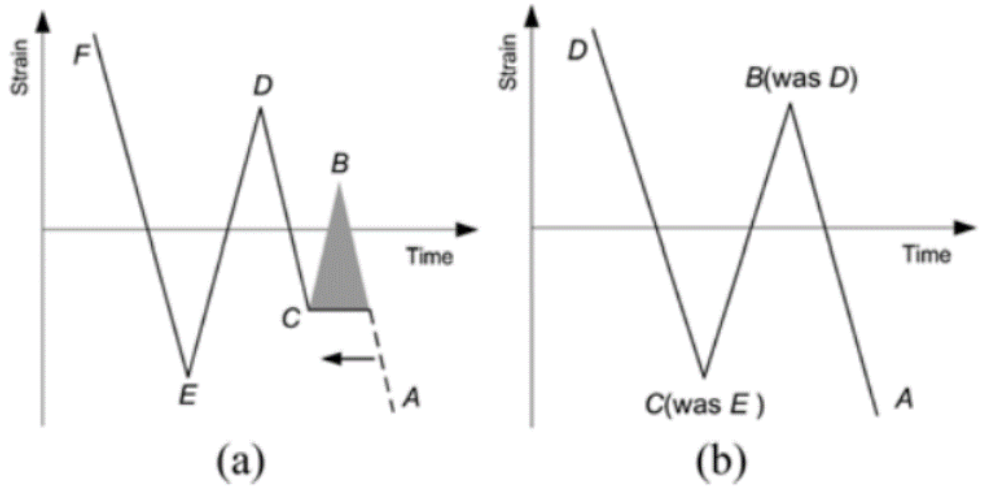

Figure 4. Rainflow Cycle Counting Procedure

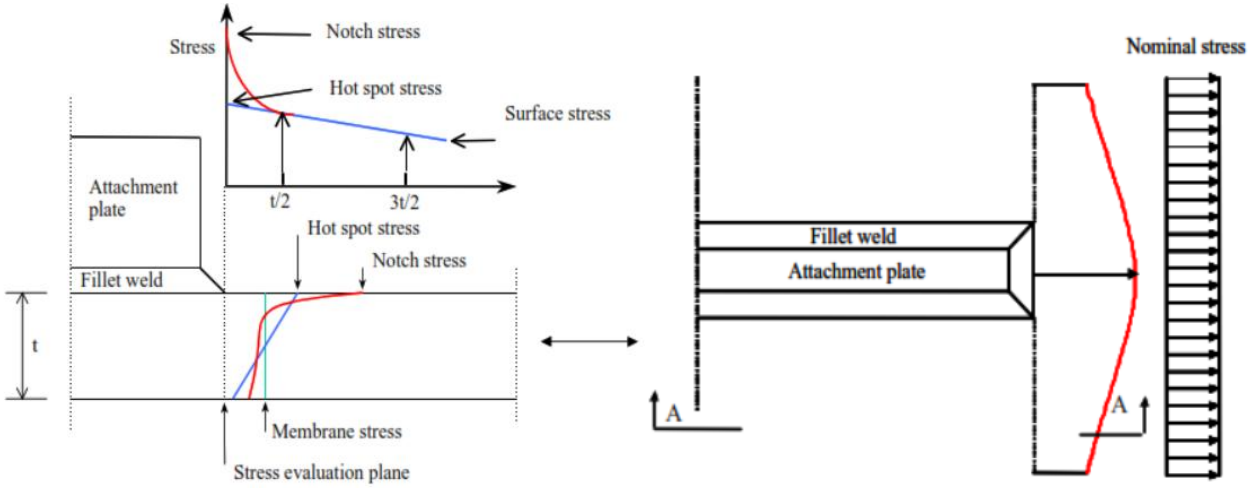

Figure 5. Illustration of Hotspot Stress Derivation

The S-N curve that will used in this study is the S-N curve for seawater environment with cathodic protection. Referring to [23], in fatigue analysis based on hotspot stress it is recommended to relate it to the D-curve on the S-N curve.

Estimating the fatigue life of a structure at the design stage is important to achieve feasibility and cost effectiveness considering the limited operational life of the structure [25]. Fatigue analysis using the S-N curve method on structural joints is carried out based on the Palmgren-Miner failure law (miner's rule). According to [26], miners' rule is a cumulative hypothesis of damage based on the concept of strain energy. The concept of strain energy states that damage occurs when the total strain energy in cycles (n) of variable amplitude loading is equal to the total of N cycles of constant amplitude loading.

The following is the cumulative damage equation based on the Palmgren-Miner law:

$$\boldsymbol{D} = \sum_{i=1}^{k} \frac{\boldsymbol{n_i}}{\boldsymbol{N_i}} \tag{5}$$

Where:

$\boldsymbol{D}$ = Damage ratio.

$\boldsymbol{n_i}$ = The number of cycles in the Si stress range that actually occur in the structure.

$\boldsymbol{N_i}$ = The number of cycles in the Si stress range obtained from the S-N curve.

The Palmgren-Miner equation assumes that the fatigue failure occurs at D = 1. Then the fatigue life can be calculated using the following equation:

$$\boldsymbol{L} = {}^{\boldsymbol{L_0}}/_{\boldsymbol{D}} \tag{6}$$

Where:

$\boldsymbol{L}$ = Fatigue life of the structure.

$\boldsymbol{L_0}$ = Time of the total number of cycles of the stress range that occurs (n_0).

III. Results and Discussion

A. Mooring System and Marine Hoses Modeling

The entire mooring system and marine hoses were modeled using a dynamic simulation software. This modeling will be based on existing field conditions, as illustrated in Figure 1. The modeling results of the entire mooring system and marine hoses during buoy stand-

alone condition and normal lifting operation can be seen in Figure 6.

B. Determining Load Case Variations for Time Domain Simulation

In this study, the fatigue life calculation for the MWB structure will use a deterministic method, hence in the cyclic load analysis, regular wave types will be used with variations in the wave direction referring to wave scatter data as presented in Table 6. Considering that it is impractical to analyze all possible wave conditions, only representative conditions are selected as the basis for the analysis.

In addition to the above, determining the load case variations for the cyclic load analysis of the MWB structure will also consider operating scenarios that refer to actual conditions. As previously explained, there are two operational modes to be analyzed: stand-alone buoy conditions (without a vessel moored at SPM #4) and normal lifting operations. The annual probability of occurrence of each operational mode is determined as follows:

- Buoy Stand-Alone Condition: 85,00%
- Normal Lifting Operation: 15.00% (assuming there are 30 lifting activities per year, with a duration of 2 days for each lifting activity)

Based on the explanation above, in total there are 154 cases that will be simulated in the time domain, which in general can be seen in the Table 7 below.

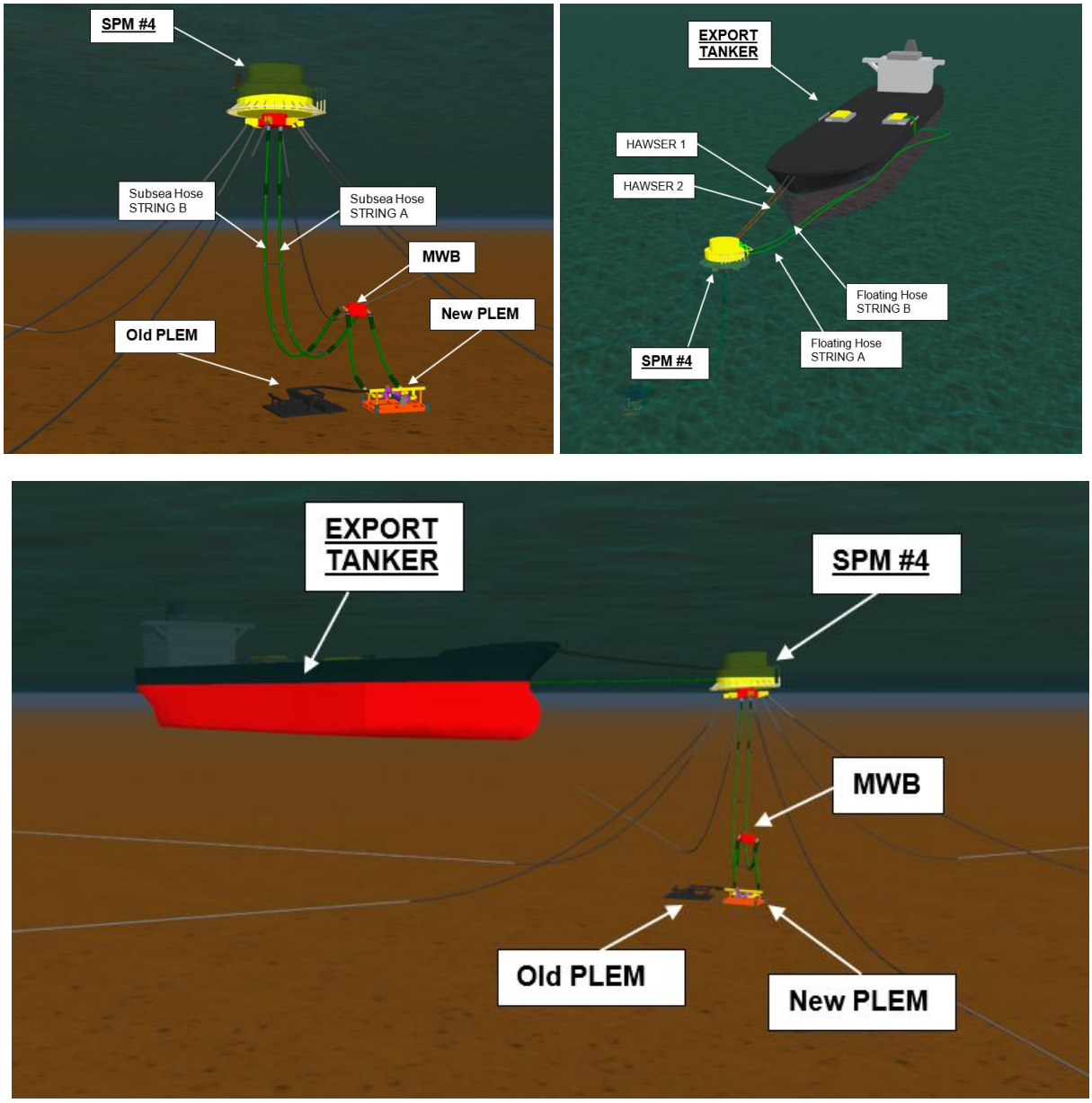

Figure 6. Mooring System and Marine Hoses Modeling

TABLE 7.
LOAD CASE VARIATION FOR TIME DOMAIN SIMULATION

No	Code	Export Tanker Loading Condition	Angular Separation of Wave, Wind, & Current	Environment Heading Direction	H [m]	T [s]	Wind Speed [m/s]	Current Speed [m/s]	Annual Probability of Occurrence [%]
			A) BUOY STAND-ALONE CONDITION						
1	LC-F1-E	Export Tanker not connected to SPM #4	Colinear	E	0.1250	2.50	12.30	0.72	15.6961%
2	LC-F2-E			E	0.3750	2.50			14.7462%
3	LC-F3-E			E	0.6250	3.50			7.3678%
4	LC-F4-E			E	0.8750	4.50			3.3069%
5	LC-F5-E			E	1.1250	4.50			1.4363%
⋮	⋮			⋮	⋮	⋮			⋮
73	LC-F73-NE			NE	0.6250	3.50			0.2239%
74	LC-F74-NE			NE	0.8750	4.50			0.0456%
75	LC-F75-NE			NE	1.1250	4.50			0.0116%
76	LC-F76-NE			NE	1.3750	4.50			0.0039%
77	LC-F77-NE			NE	1.6250	4.50			0.0010%
						Sum of Annual Probability A)			85.00%
			B) NORMAL LIFTING OPERATION						
78	LC-F78-E	Full Load Condition (98 %)	Colinear	E	0.1250	2.50	12.30	0.72	2.7699%
79	LC-F79-E			E	0.3750	2.50			2.6023%
80	LC-F80-E			E	0.6250	3.50			1.3002%
81	LC-F81-E			E	0.8750	4.50			0.5836%
82	LC-F82-E			E	1.1250	4.50			0.2535%
⋮	⋮			⋮	⋮	⋮			⋮
150	LC-F150-NE			NE	0.6250	3.50			0.0395%
151	LC-F151-NE			NE	0.8750	4.50			0.0080%
152	LC-F152-NE			NE	1.1250	4.50			0.0021%
153	LC-F153-NE			NE	1.3750	4.50			0.0007%
154	LC-F154-NE			NE	1.6250	4.50			0.0002%
						Sum of Annual Probability B)			15.00%

C. Time Domain Simulation and Rainflow Counting

To obtain the magnitude of the cyclic load acting on the MWB structure, a time domain simulation will be carried out utilizing the modeling results of the entire mooring system and marine hoses series, as well as variations in load cases based on operational scenarios as explained above. For each load case, a time domain simulation will be carried out with a duration of 3 hours (10,800 seconds), this period is considered representative enough to describe the dynamic behavior of the system and has also referred to [17].explained above. For each load case, a time domain simulation will be carried out with a duration of 3 hours (10,800 seconds), this period is considered representative enough to describe the dynamic behavior of the system and has also referred to [17].

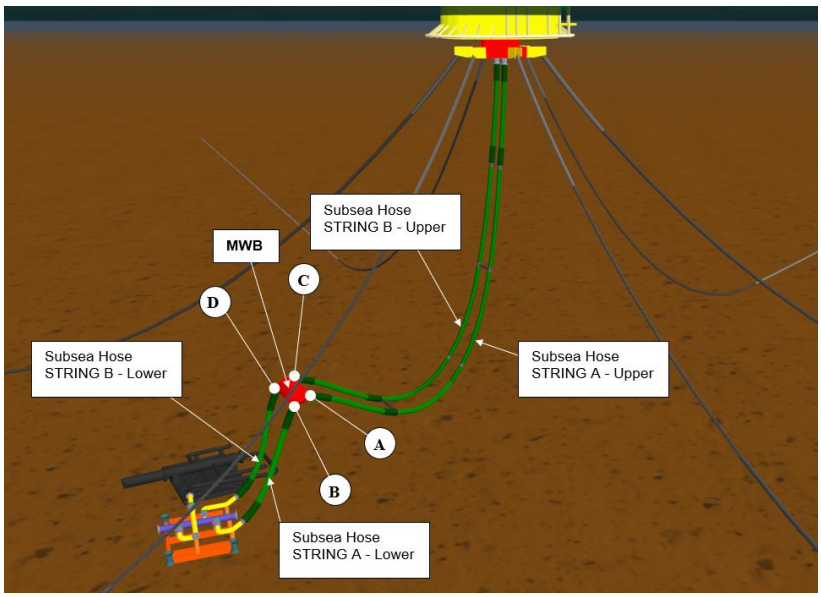

Figure 7. Illustration for Cyclic Load Extraction Location for MWB

TABLE 8.
CYCLIC LOAD EXTRACTION LOCATIONS FOR MWB

Code	Location where cyclic loads will be extracted
A	Connection between MWB and Subsea Hose STRING A – Upper
B	Connection between MWB and Subsea Hose STRING A – Lower
C	Connection between MWB and Subsea Hose STRING B – Upper
D	Connection between MWB and Subsea Hose STRING B – Lower

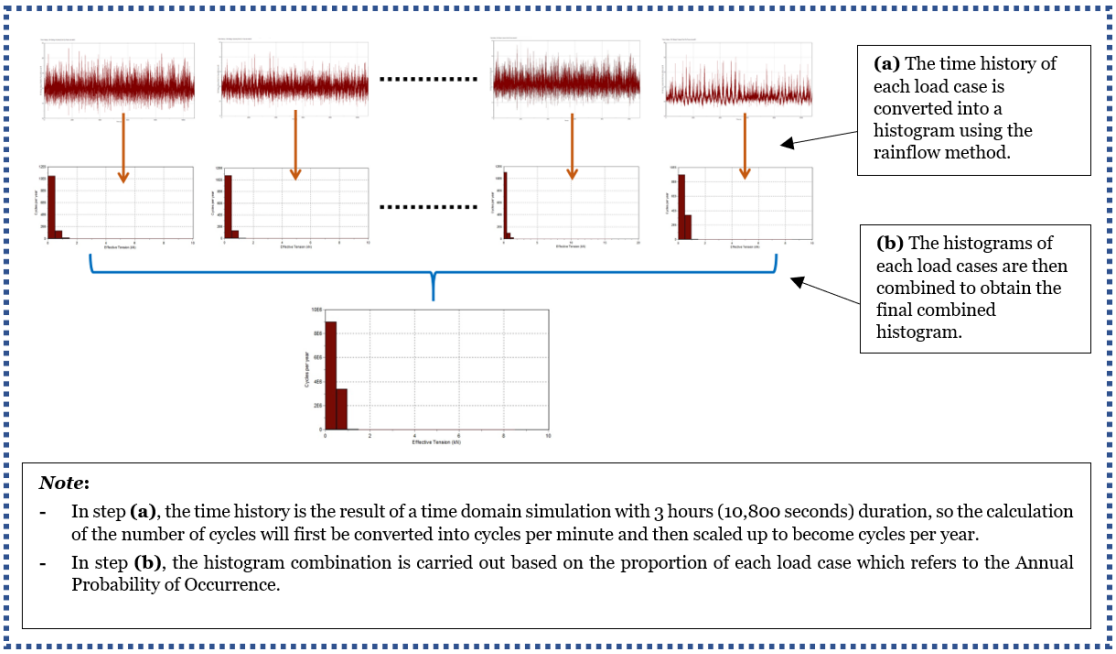

Figure 8. Illustration of the Cycle Count Calculation Process

As part of the fatigue analysis process, specific locations for cyclic load extraction were determined. These locations represent the connection points between the MWB and the subsea hose. Details of the extraction locations for the cyclic loads acting on the MWB are shown in Figure 7 and Table 8 below.

The main output of this simulation is the time history of the tension that occurs at the connection location between the MWB and the subsea hose (Figure 7 and Table 8) for each load case variation. After all the time history data is obtained, the number of cycles is calculated using the rainflow cycle counting method. The purpose of this calculation is to determine the tension range and the number of cycles per year experienced by each connection. The rainflow cycle counting method used in this study follows a standard algoritm commonly used in fatigue analysis, which is already, which is already available in the dynamic simulation software

The result of the rainflow cycle counting process is a histogram showing the distribution of the number of cycles against the tension range during the simulation duration. This will produce a histogram for each connection location in each load case. The next step is to combine and calibrate all the histograms using the Annual Probability of Occurrence (see Table 7) for each load case. With this process, the individual histograms can be combined and scaled to produce a total number of cycles per year for each location, which will then be used as input for the fatigue analysis of the MWB structure. The process of calculating the number of cycles as explained above is illustrated in Figure 8.

The results of the cyclic load calculations in the form of a combined histogram can be seen in Figure 9. By considering 2 (two) operational scenarios, namely normal lifting operations and stand-alone buoy conditions, it was found that the distribution of cyclic loads acting on the MWB structure varies with the magnitude of the tension range value ranging from 0.5 kN to 8.5 kN. Meanwhile, the frequency of each tension range value is dominated by a small value range (namely 0.5 kN) with a frequency of occurrence reaching 11,051,967 cycles per year.

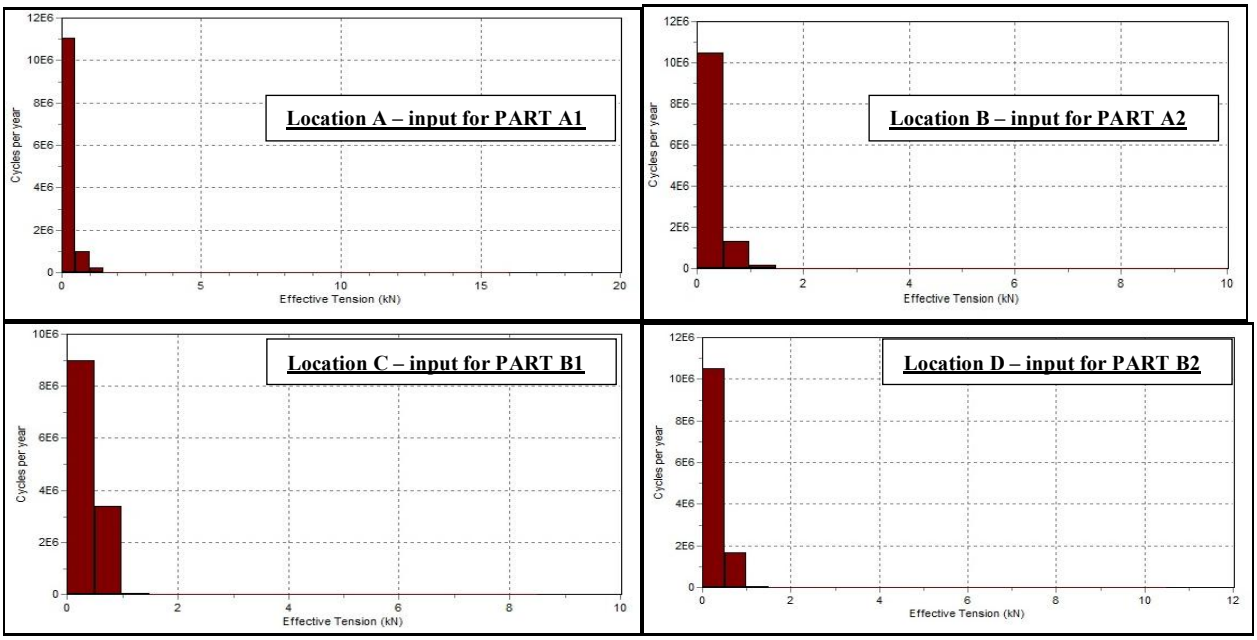

Figure. 9. Cycle Counting Calculation Result

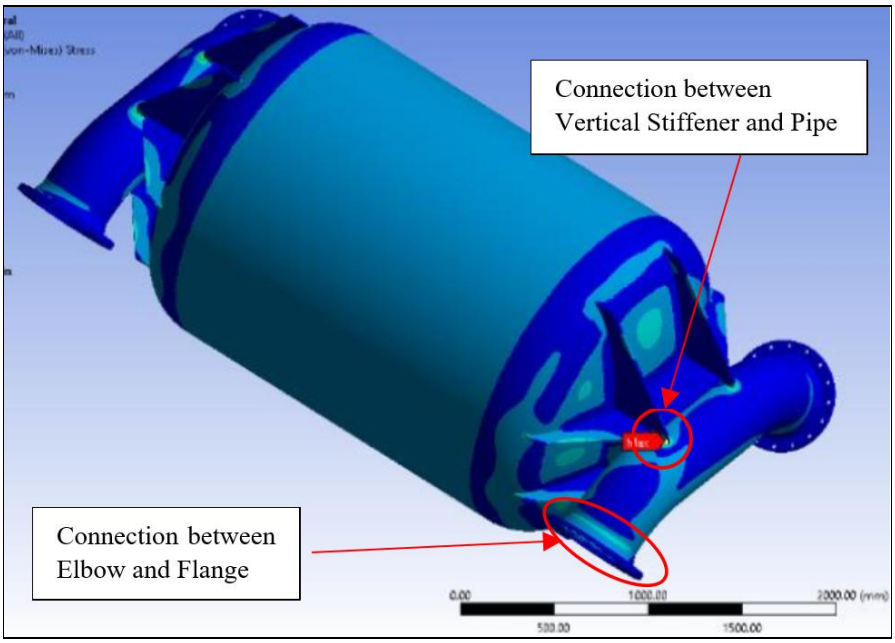

Figure. 10. Global Stress Distribution on MWB Structures

D. Identification of Critical Areas in Mid-Water Buoy (MWB) Structures

Local stresses are determined by assuming that the material behaves in a linear manner and by using a simplified structural model that doesn't include real-world construction variations. The area covered by the local model needs to be selected so that the influence of the boundaries on the parts being studied is minimal, making it easier to set up suitable boundary conditions.

Critical areas in a structure are generally located at joints, where stress concentrations occur. To accurately determine the location of critical areas, a global stress distribution of the MWB structure is required. In this study, the global stress distribution of the MWB will refer to the results of a global strength analysis for MWB structures that have been conducted in [27]. The global stress distribution for MWB structure is shown in Figure 10. Based on the explanation above and based on the global stress distribution in Figure 10, the critical areas that have been identified are as follows:

- **Connection between Vertical Stiffener and Pipe**
- **Connection between Elbow and Flange**

Furthermore, the local modeling performed must be able to cover all the critical areas mentioned above. Therefore, the local modeling for the MWB structure will be divided into 4 (four) parts, as illustrated in Figure 11.

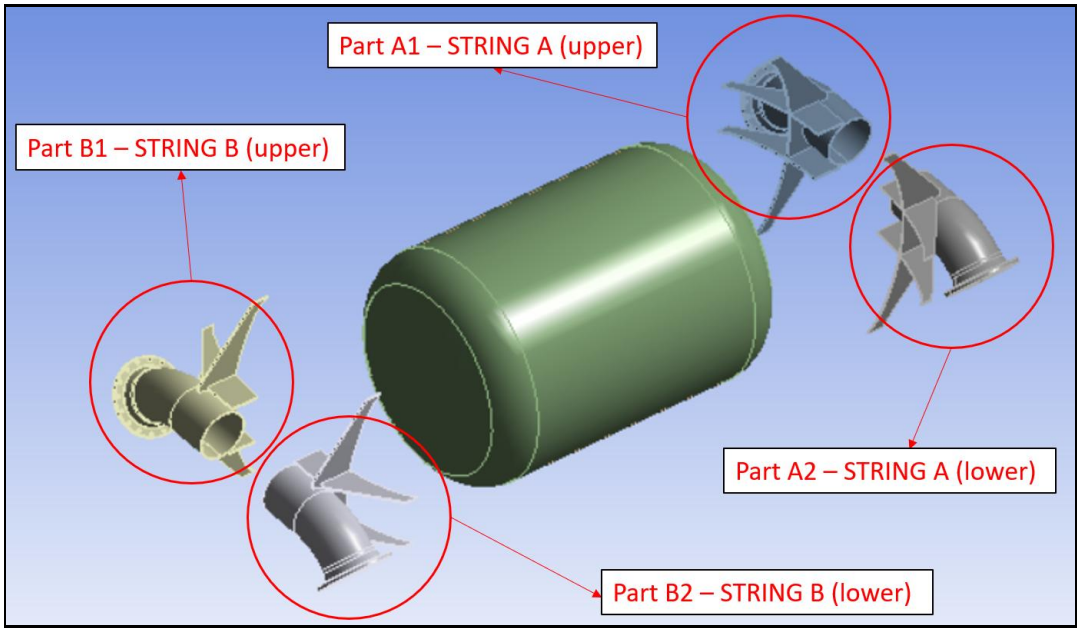

Figure. 11. Extent for Local Structure Modeling of MWB

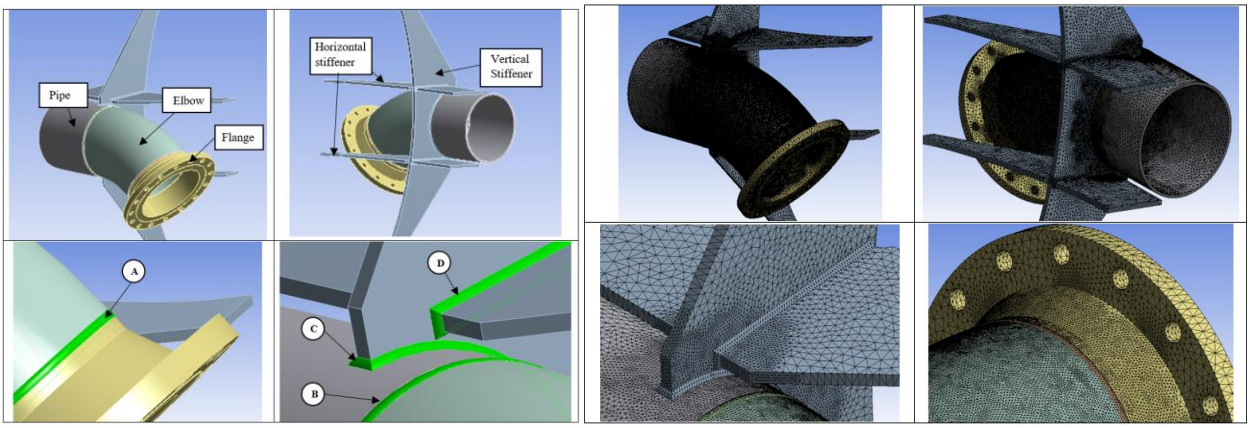

Figure. 12. Local Structure Modeling and Meshing on Critical Area of MWB

TABLE 9.
DETAILS OF WELDING TYPES AND SIZES IN CRITICAL AREAS OF MWB

Code	Location of Weld Connection	Weld Type	Weld Size	Mesh Size
A	Between Elbow and Flange	Butt Weld – Single V Groove	6 mm	4 mm
B	Between Pipe and Elbow	Butt Weld – Single V Groove	6 mm	4 mm
C	Between Vertical Stiffener and Pipe	Double Bevel + Fillet Weld	6 mm	4 mm
D	Between Vertical Stiffener and Horizontal Stiffener	Double Bevel + Fillet Weld	6 mm	4 mm
-	Global Mesh Size			8 mm

E. 3D Geometry Modeling for Critical Areas of Mid-Water Buoy (MWB) Structures

3D geometric modeling for critical areas in the MWB structure will include stiffener and piping components. Since the 4 (four) parts mentioned above are symmetrical and identical, modeling will be performed for only 1 (one) part, or alternatively, all parts will use the same model. The modeling results can be seen in the Figure 12. All components are modeled using **solid elements** and involving **weld toe**. An explanation of the type and size of the weld toe modeled for each connection can be seen in Table 9.

All components of the MWB structure are modeled as linear elastic materials, which can be defined through 2 (two) properties, Young's Modulus (E) and Poisson's ratio (v).

The meshing process is a crucial step in structural analysis using the Finite Element Method (FEM) approach, as it directly affects the accuracy of the stress results. In this study, the meshing process for the critical areas of the MWB structure was performed using a Finite Element Analysis (FEA) software, employing solid element types suitable for complex geometries requiring high precision.

Element sizing was carried out in stages, starting with global element sizing and continuing with local mesh refinement in critical areas. Furthermore, mesh convergence was checked to ensure that the selected

element sizes produced stable stress values and no longer varied significantly with changes in mesh size.

Based on the iterations performed, the element size in critical areas was reduced to 4 mm, while in non-critical areas it was maintained at 8 mm. With these element sizes, a dense element distribution was achieved in critical areas, with a total of around 950,000 elements, resulting in efficient and accurate simulations in the focus areas of the analysis. The details of the mesh sizes used are also described in Table 9.

F. Boundary Condition for Local Structural Analysis

To obtain FEM analysis results that are representative of the actual conditions of the MWB structure, boundary conditions must be accurately determined to reflect operational characteristics and environmental conditions. The illustration of the boundary condition that applied to the model is presented in Figure 9. The explanation of these boundary conditions presented in several points below:

(a) *Fixed support*

In local structural analysis, particularly using the FEM approach, fixed support boundary conditions are applied to the model's boundary surfaces representing connections to the larger (global) structure. This application aims to represent the relative stiffness of structural parts not directly modeled in the local analysis but still subject to loading and restraint. By applying fixed support, all degrees of freedom, both translational and rotational, on the boundary surfaces are locked, preventing displacement.

In addition to the above, the application of fixed support to the local model also serves to ensure numerical stability and allows for focused analysis of local stress distribution without being affected by global deformation.

(b) *Self-Structural Weight (Standard Earth Gravity*

The load due to the self-structural weight acting on a structure is calculated using the following equation:

$$\boldsymbol{F = m.g} \tag{2}$$

Where:
$\boldsymbol{F}$ = Gravitational force (N)
$\boldsymbol{m}$ = Mass of the structure (Kg)
$\boldsymbol{g}$ = Acceleration due to gravity (9.8066 m/s²)

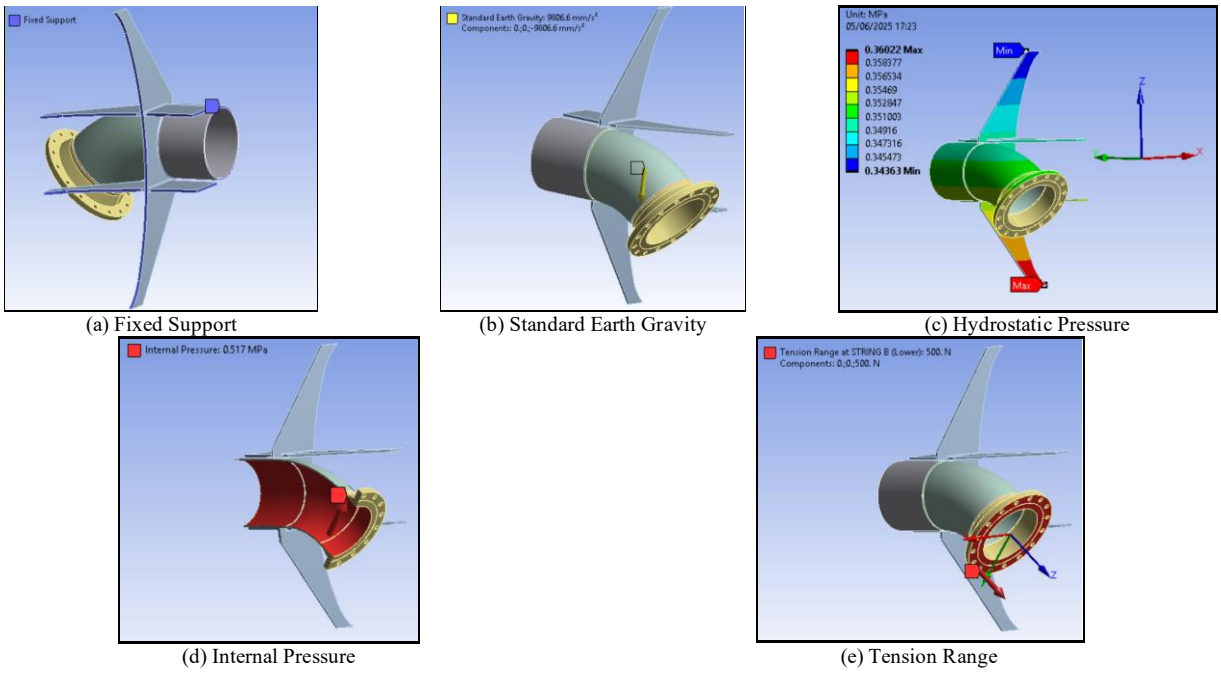

(a) Fixed Support (b) Standard Earth Gravity (c) Hydrostatic Pressure

(d) Internal Pressure (e) Tension Range

Figure 9. Application of Boundary Condition for Local Model

(c) Internal Pressure

For fatigue analysis purposes, the internal pressure applied to the model will be based on the Maximum Allowable Operating Pressure (MAOP) value of 0.517 MPa. This pressure is applied to the inner surface of the piping component.

(d) Hydrostatic Pressure

Hydrostatic pressure is the pressure exerted by a fluid at equilibrium due to the force of gravity. The value of hydrostatic pressure increases with depth according to the following equation:

$$\boldsymbol{P = \rho g h} \tag{2}$$

Where:
$\boldsymbol{P}$ = Hydrostatic pressure (N)
$\boldsymbol{\rho}$ = Fluid density (Kg/m^3)
$\boldsymbol{g}$ = Acceleration due to gravity (9.8066 m/s²)
$\boldsymbol{h}$ = Depth below the water surface (m)

Figure 10. Stress Path for Derivation of Hotspot Stress

TABLE 10.
LOADCASE VARIATION FOR HOTSPOT STRESS CALCULATION

No	Load Case Code	Part of MWB	Tension Range (kN)	Cycles per year	Internal Pressure	External Pressure
1	MWB-H1	**PART A1** (Part of MWB which connected to Subsea Hose STRING A -Upper	5	11,051,967	0.517 MPa (Maximum Allowable Operating Pressure)	Hydrostatic Pressure at 32.5 m Water Depth
2	MWB-H2		1.00	1,012,264		
⋮	⋮		⋮	⋮		
15	MWB-H15		7.50	67		
16	MWB-H16		8.00	38		
17	MWB-H17	**PART A2** (Part of MWB which connected to Subsea Hose STRING A -Lower	0.50	10,458,431	0.517 MPa (Maximum Allowable Operating Pressure)	Hydrostatic Pressure at 32.5 m Water Depth
18	MWB-H18		1.00	1,307,555		
⋮	⋮		⋮	⋮		
29	MWB-H29		6.50	3		
30	MWB-H30		7.00	1		
31	MWB-H31	**PART B1** (Part of MWB which connected to Subsea Hose STRING B -Upper	0.50	8,971,813	0.517 MPa (Maximum Allowable Operating Pressure)	Hydrostatic Pressure at 32.5 m Water Depth
32	MWB-H32		1.00	3,375,372		
⋮	⋮		⋮	⋮		
42	MWB-H42		8.00	97		
43	MWB-H43		8.50	7		
44	MWB-H44	**PART B2** (Part of MWB which connected to Subsea Hose STRING B -Lower	0.50	10,499,204	0.517 MPa (Maximum Allowable Operating Pressure)	Hydrostatic Pressure at 32.5 m Water Depth
45	MWB-H45		1.00	1,670,200		
⋮	⋮		⋮	⋮		
56	MWB-H56		6.50	32		
57	MWB-H57		7.00	1		

(e) Cyclic Load (Tension Range)

Cyclic loads in the form of tension ranges resulting from the dynamics of subsea hose movement will be applied to the surface of the flange component, where the surface is the interface area between the MWB structure and the subsea hose. The magnitude of the cyclic load will be varied by referring to the cyclic load analysis results as presented in Figure 9.

G. Hotspot Stress Analysis

As explained previously, the hotspot stress analysis begins with the determination of the load cases to be used in the analysis. The load case variations for the hotspot stress analysis are determined based on the results of the cyclic load analysis as shown in Figure 9, which indicates that the cyclic loads acting on each part (see Figure 11) are different. These cyclic loads are then combined with the boundary conditions specified in

Figure 9. The load case variations for the hotspot stress analysis can be seen in Table 10.

For hotspot stress calculations, the stress components on the plate surface are evaluated along the stress path as shown in Figure 14, then extrapolated to the hotspot location. The extrapolation process is carried out using the average stress value between adjacent elements. The stress evaluation points are recommended to be at a distance of 0.5 *t* and 1.5 *t* from the hotspot point, where *t* is the plate thickness at the weld toe location. These points are also known as stress read-out points.

The equation for effective hotspot stress, equation (3), considers the possibility of fatigue cracking in the weld toe area, especially if the principal stress direction is parallel to the weld toe direction. The principal stress will be obtained from a static-structural analysis using FEM based on the local structure model, meshing, boundary conditions, and load case variation that have been described previously.

The hotspot stress analysis result for critical area of MWB structure is presented in Table 11. In this study, the hotspot analysis result is presented only for PART A1. Based on the analysis result, it was found that the effective hotspot stress range (σ_{eff}) for the connection between the vertical stiffener and the pipe ranged from 18.51 MPa to 23.83 MPa. Meanwhile, for the connection between the elbow and flange, it ranged from 6.01 MPa to 6.51 MPa.

H. Fatigue Life Calculation

In accordance with the explanations and theoretical basis discussed previously, the fatigue life calculation for critical areas of the MWB structure is performed using a deterministic approach and utilizing the S-N curve from [23]. The local stresses used in the fatigue life calculation will utilize hotspot stress.

TABLE 11.
HOTSPOT STRESS CALCULATION RESULT FOR PART A1

Load Case Code	Location of Stress Read-Out Point	Stress Read-Out Value [MPa]		Extrapolated Effective Hotspot Stress Range, σ_{eff} [MPa]
		1.5 t from weld toe	0.5 t from weld toe	
MWB-H1	Connection between Vertical Stiffener and Pipe	13.45	18.20	18.51
	Connection between Elbow and Flange	10.82	8.06	6.01
MWB-H2	Connection between Vertical Stiffener and Pipe	13.67	18.52	18.85
	Connection between Elbow and Flange	10.94	8.12	6.03
MWB-H3	Connection between Vertical Stiffener and Pipe	13.89	18.84	19.18
	Connection between Elbow and Flange	11.06	8.17	6.05
MWB-H4	Connection between Vertical Stiffener and Pipe	14.11	19.16	19.51
	Connection between Elbow and Flange	11.18	8.23	6.08
MWB-H5	Connection between Vertical Stiffener and Pipe	14.33	19.47	19.84
	Connection between Elbow and Flange	11.29	8.28	6.10
MWB-H6	Connection between Vertical Stiffener and Pipe	14.55	19.79	20.18
	Connection between Elbow and Flange	11.41	8.34	6.12
MWB-H7	Connection between Vertical Stiffener and Pipe	14.77	20.11	20.51
	Connection between Elbow and Flange	11.53	8.40	6.15
MWB-H8	Connection between Vertical Stiffener and Pipe	14.99	20.43	20.84
	Connection between Elbow and Flange	11.65	8.46	6.17
MWB-H9	Connection between Vertical Stiffener and Pipe	15.21	20.75	21.17
	Connection between Elbow and Flange	11.77	8.52	6.20
MWB-H10	Connection between Vertical Stiffener and Pipe	15.43	21.07	21.50
	Connection between Elbow and Flange	11.89	8.58	6.23
MWB-H11	Connection between Vertical Stiffener and Pipe	15.65	21.39	21.84
	Connection between Elbow and Flange	12.01	8.64	6.27
MWB-H12	Connection between Vertical Stiffener and Pipe	15.87	21.71	22.17
	Connection between Elbow and Flange	12.12	8.71	6.30
MWB-H13	Connection between Vertical Stiffener and Pipe	16.09	22.03	22.50
	Connection between Elbow and Flange	12.24	8.78	6.34
MWB-H14	Connection between Vertical Stiffener and Pipe	16.31	22.35	22.83
	Connection between Elbow and Flange	12.36	8.85	6.38
MWB-H15	Connection between Vertical Stiffener and Pipe	16.53	22.67	23.17
	Connection between Elbow and Flange	12.48	8.92	6.42
MWB-H16	Connection between Vertical Stiffener and Pipe	16.76	22.99	23.50
	Connection between Elbow and Flange	12.60	8.99	6.47

It should be noted that the MWB structure has been designed with cathodic protection, therefore the S-N curve used in the design is the S-N curve for a sea water environment with cathodic protection. Furthermore, referring to [23], it is recommended to use the **D-curve** in fatigue life calculations using the hotspot stress method. The parameters for the D-curve used in the calculation are shown in Table 12.

Next, the damage ratio ($\mathbf{D_i}$) for each effective hotspot stress range ($\boldsymbol{\sigma_{eff}}$) will be calculated using the Palmgren-Miner rules by applying equation (5). The $\mathbf{n_i}$ value for each effective stress range will use the number of cycles per year obtained from Table 11. Meanwhile, the $\mathbf{N_i}$ value is obtained by inputting the effective hotspot stress range value ($\boldsymbol{\sigma_{eff}}$) that obtained from Table 11 and the D-curve parameter values into the equation (4). With the steps above, the annual damage ratio value ($\mathbf{D} = \sum \mathbf{D_i}$) will be obtained.

By obtaining the annual damage ratio value (D), the fatigue life prediction for the MWB structure can be obtained using equation (6). The details of the fatigue life calculation for PART A1 is presented in Table 13. Meanwhile, the summary of the fatigue life calculation results for all parts (PART A1 until Part B2) is presented in the Table 14.

Based on the fatigue calculation result in Table 14, it was found that the fatigue life of MWB structure for the connection between the vertical stiffener and the pipe ranged from 145.93 years to 153.35 years with annual damage ratio ranged from 0.0065 to 0.0069. Meanwhile, for the connection between the elbow and flange, the fatigue life ranged from 41,226.98 years to 42,881.84 years with the value of annual damage ratio ranged from 0.0000233 to 0.000024.

TABLE 12.
S-N CURVE PARAMETER FOR D-CURVE

Parameter	Value
m_1	3.0
$\log \bar{a}_1$	11.764
m_2	5.0
$\log \bar{a}_2$	15.606
Fatigue limit at 10^7 cycles	52.63

TABLE 13.
FATIGUE LIFE CALCULATION FOR CONNECTION BETWEEN VERTICAL STIFFENER AND PIPE OF PART A1

Effective Hotspot Stress Range, σ_{eff} [Mpa]	Cycle per Year, n_i [cycles]	m_1	$\log a_1$	m_2	$\log a_2$	$\log N_i$	N_i	Damage Ratio $D_i = n_i / N_i$
18.51	1.11.E+07	3	11.764	5	15.606	9.27	1.86.E+09	5.96.E-03
18.85	1.01.E+06	3	11.764	5	15.606	9.23	1.70.E+09	5.96.E-04
19.18	2.46.E+05	3	11.764	5	15.606	9.19	1.56.E+09	1.58.E-04
19.51	2.18.E+03	3	11.764	5	15.606	9.15	1.43.E+09	1.53.E-06
19.84	1.03.E+03	3	11.764	5	15.606	9.12	1.31.E+09	7.86.E-07
20.18	1.30.E+02	3	11.764	5	15.606	9.08	1.21.E+09	1.07.E-07
20.51	1.10.E+02	3	11.764	5	15.606	9.05	1.11.E+09	9.89.E-08
20.84	2.78.E+02	3	11.764	5	15.606	9.01	1.03.E+09	2.71.E-07
21.17	3.84.E+01	3	11.764	5	15.606	8.98	9.49.E+08	4.05.E-08
21.50	1.23.E+02	3	11.764	5	15.606	8.94	8.78.E+08	1.40.E-07
21.84	3.95.E+00	3	11.764	5	15.606	8.91	8.13.E+08	4.86.E-09
22.17	6.25.E-01	3	11.764	5	15.606	8.88	7.54.E+08	8.29.E-10
22.50	5.47.E-01	3	11.764	5	15.606	8.84	7.00.E+08	7.82.E-10
22.83	7.88.E-01	3	11.764	5	15.606	8.81	6.50.E+08	1.21.E-09
23.17	6.71.E+01	3	11.764	5	15.606	8.78	6.05.E+08	1.11.E-07
23.50	3.79.E+01	3	11.764	5	15.606	8.75	5.63.E+08	6.72.E-08
							Annual Damage Ratio, D = $\sum D_i$	0.0067
							Fatigue Life = 1/D [Years]	148.93

TABLE 14.
SUMMARY OF FATIGUE LIFE CALCULATION

Part of MWB	Location of Critical Areas	Annual Damage Ratio	Fatigue Life [years]
PART A1	Connection between Vertical Stiffener and Pipe	0.0067	148.93
	Connection between Elbow and Flange	0.0000240	41592.90
PART A2	Connection between Vertical Stiffener and Pipe	0.0065	153.35
	Connection between Elbow and Flange	0.0000233	42881.84
PART B1	Connection between Vertical Stiffener and Pipe	0.0069	145.93
	Connection between Elbow and Flange	0.0000243	41226.98
PART B2	Connection between Vertical Stiffener and Pipe	0.0067	149.68
	Connection between Elbow and Flange	0.0000239	41870.41

IV. CONCLUSION

Based on the entire series of analyses and discussions that have been carried out, it can be concluded that the lowest fatigue life value of MWB structure is occurs at PART B1 (the part of the MWB connected to the Subsea Hose STRING B – Upper) with value of 145.93 years and with annual damage ratio of 0.0069 for Connection between the Vertical Stiffener and the Pipe.

The results of the analysis above can be used as a reference to assess the remaining life of the MWB structure and can also be used as a guideline in preparing maintenance and inspection plans.

ACKNOWLEDGEMENTS

Thank you to PT. Citra Mas for the assistance and support provided in completing this research.

REFERENCES

[1] R. Rachmadi and E. Puspitawati, "Impact of Belt Road Initiative on Indonesia's Oil and Gas Trade," Journal of International

Studies on Energy Affairs, vol. 3, no. 1, pp. 1–16, Jun. 2022, doi: 10.51413/jisea.vol3.iss1.2022.1-16.

[2] J. Kusuma, K. B. Artana, and A. A. B. Dinariyana, "Market Analysis of Natural Gas Supply and Demand in East Java Province to Enable a Sustainable Scenario Using System Dynamics Simulation," in IOP Conference Series: Earth and Environmental Science, IOP Publishing Ltd, Sep. 2020. doi: 10.1088/1755-1315/557/1/012041.

[3] E. J. B. Ribeiro and C. Bartz, "Tubarao Martelo Field Development: Lazy S Riser Configuration Using Mid Water Arch (MWA)," in Proceedings of the ASME 2015 34th International Conference on Ocean, Offshore and Arctic Engineering OMAE2015, Newfoundland, 2015. [Online]. Available: http://www.asme.org/abo

[4] IACS, "UR L5: Computer Software for Onboard Stability Calculations," 2020.

[5] E. B. Djatmiko, Perilaku dan Operabilitas Bangunan Laut di Atas Gelombang Acak. Surabaya: ITS PRESS, 2012. [Online]. Available: https://www.researchgate.net/publication/335620271

[6] C. V. Amaechi, F. Wang, and J. Ye, "Numerical studies on CALM buoy motion responses and the effect of buoy geometry cum skirt dimensions with its hydrodynamic waves-current interactions," Ocean Engineering, vol. 244, Jan. 2022, doi: 10.1016/j.oceaneng.2021.110378.

[7] J. Wichers, Guide to Single Point Moorings. Houston: WMooring, Inc, 2013.

[8] Angelo. Luongo and Daniele. Zulli, Mathematical Models of Beams and Cables. London and Hoboken: ISTE Ltd - John Wiley & Sons, Inc., 2013.

[9] H. Max. Irvine, Cable Structures. Massachussetts: MIT Press, 1981.

[10] O. M. Faltinsen, Sea Loads on Ships and Offshore Structures. New York: Cambridge University Press, 1990.

[11] C. V. Amaechi, F. Wang, and J. Ye, "Investigation on Hydrodynamic Characteristics, Wave–Current Interaction and Sensitivity Analysis of Submarine Hoses Attached to a CALM Buoy," J Mar Sci Eng, vol. 10, no. 1, Jan. 2022, doi: 10.3390/jmse10010120.

[12] K. Anderson and M. O'Connor, "The Evolution of Lazy-S Flexible Riser Configuration Design for Harsh Environment," in Proceedings of the ASME 2012 31st International Conference on Ocean, Offshore and Arctic Engineering OMAE2012, Rio de Janeiro, 2012. [Online]. Available: http://www.asme.org/about-asme/terms-of-use

[13] C. Russell and B. Vignaud, "Hydrodynamic Loading on Mid Water Arch Structures," in Proceedings of the ASME 2011 30th International Conference on Ocean, Offshore and Arctic Engineering OMAE2011, Rotterdam, 2011. [Online]. Available: http://proceedings.asmedigitalcollection.asme.org/pdfaccess.ashx?url=/data/conferences/omae2011/69570/

[14] API, "17L1: Specification for Flexible Pipe Ancillary Equipment," 2013.

[15] J. Hill, S. Laycock, S. Chai, C. Balash, and H. Morand, "Hydrodynamic loads and response of a Mid Water Arch structure," Ocean Engineering, vol. 83, pp. 76–86, Jun. 2014, doi: 10.1016/j.oceaneng.2014.02.032.

[16] DNV-GL, "RP-C205: Environmental conditions and environmental loads," 2019.

[17] API, "RP-2SK: Design and Analysis of Stationkeeping Systems for Floating Structures," 2005.

[18] N. E. Dowling, "Dowling (1971) - Fatigue failure predictions for complicated stress strain histories," 1971.

[19] I. Rychlik, "A new definition of the rainflow cycle counting method," Int J Fatigue, vol. 9, no. 2, pp. 119–121, 1987.

[20] C. Amzallag, J. P. Gerey, J. L. Robert1, and J. Bahuaudl, "Standardization of the rainflow counting method for fatigue analysis Preliminary treatment of the sequence," Int J Fatigue, vol. 16, no. 4, pp. 287–293, Jun. 1994, doi: https://doi.org/10.1016/0142-1123(94)90343-3.

[21] S. D. Downing and D. F. Socie, "Simple rainflow counting algorithms," Int J Fatigue, vol. 4, no. 1, Jan. 1982, doi: https://doi.org/10.1016/0142-1123(82)90018-4.

[22] ASTM, "Standard Practices for Cycle Counting in Fatigue Analysis," ASTM International, 2011. doi: 10.1520/E1049-85R11E01.

[23] DNV-GL, "RP-C203: Fatigue design of offshore steel structures," 2014. [Online]. Available: www.dnvgl.com.

[24] J. Retnamma, "Deterministic and Spectral Fatigue Analysis of Tubular Joints of a Jacket Platform," Int J Sci Eng Res, vol. 8, no. 11, 2017, [Online]. Available: http://www.ijser.org

[25] A. Almar-Næss, Fatigue Handbook: offshore steel structures. Trondheim: Tapir, 1985.

[26] B. M. Ayyub, G. J. White, T. F. Bell-Wright, and E. S. Purcell, "Reliability-Based Comparative Life Expectancy Assessment of Patrol Boat Hull Structures," 1990. [Online]. Available: https://www.researchgate.net/publication/235196929

[27] PT Citra Mas, "PROD-UR-RPT-0025 Strength Analysis of Mid-Water Buoy (MWB) Double String at SPM #4," Project Report, 2025.